

13

OPTICAL TESTING

Daniel Malacara-Hernández

*Centro de Investigaciones en Optica, A. C.
León, Gto., Mexico*

13.1 GLOSSARY

E	electric field strength
k	radian wave number
r	position
t	time
λ	wavelength
φ	phase
ω	radian frequency

13.2 INTRODUCTION

The requirements for high-quality optical surfaces are more demanding every day. They should be tested in an easier, faster, and more accurate manner. Optical surfaces usually have a flat or a spherical *shape*, but they also may be toroidal or generally aspheric. Frequently, an aspherical surface is a conic of revolution, but an aspherical surface can only be made as good as it can be tested. Here, the field of optical testing will be reviewed. There are some references that the reader may consult for further details.¹

13.3 CLASSICAL NONINTERFEROMETRIC TESTS

Some classical tests will never be obsolete, because they are cheap, simple, and provide qualitative results about the shape of the optical surface or wavefront almost instantly. These are the Foucault or knife-edge test, the Ronchi test, and the Hartmann test. They will be described next.

Foucault Test

The Foucault or knife-edge test was invented by Leon Foucault² in France, to evaluate the quality of spherical surfaces. This test described by Ojeda-Castañeda³ detects the presence of transverse aberrations by intercepting the reflected rays deviated from their ideal trajectory, as Fig. 1 shows. The observer is behind the knife, looking at the illuminated optical surface, with the reflected rays entering the eye. The regions corresponding to the intercepted rays will appear dark, as in Fig. 2.

This test is extremely sensitive. If the wavefront is nearly spherical, irregularities as small as a fraction of the wavelength of the light may be easily detected. This is the simplest and most powerful qualitative test for observing small irregularities and evaluating the general smoothness of the spherical

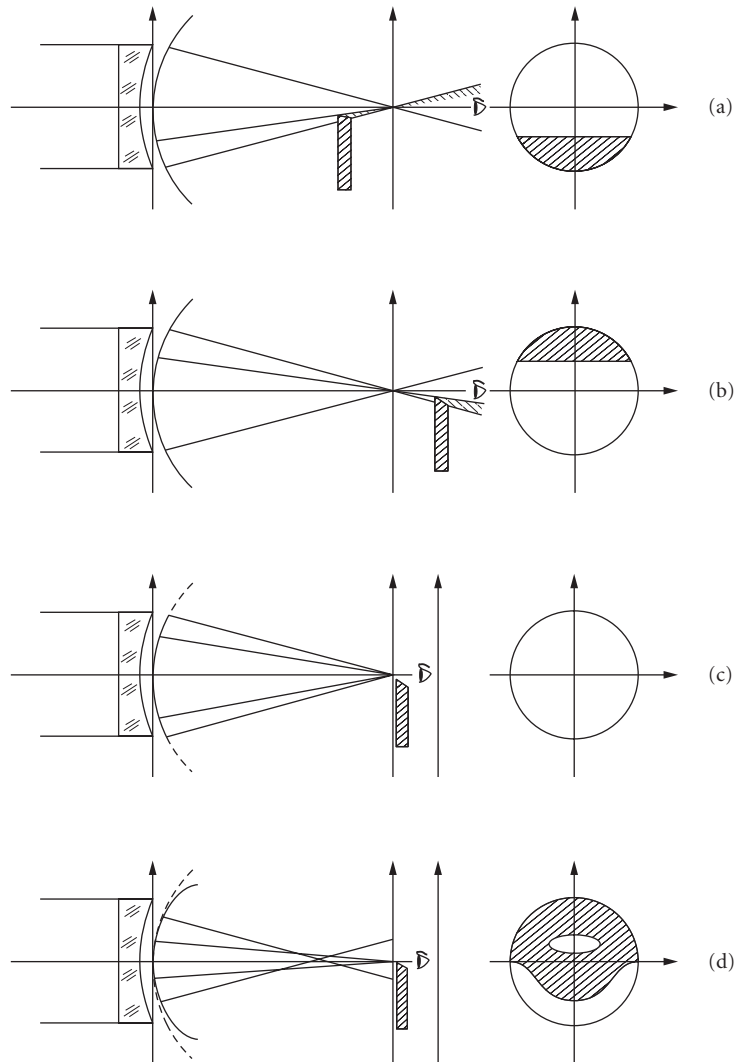


FIGURE 1 Optical schematics for the Foucault test of a spherical mirror at several positions of the knife edge.



FIGURE 2 An optical surface being examined by the Foucault test. (From Ojeda-Castañeda.³)

surface under test. Any other surface or lens may be tested, as long as it produces an almost spherical wavefront, otherwise, an aberration compensator must be used, as will be described later. Very often a razor blade makes a good, straight, sharp edge that is large enough to cover the focal region.

Ronchi Test

Vasco Ronchi⁴ invented his famous test in Italy in 1923. A coarse ruling (50–100 lines per inch) is placed in the convergent light beam reflected from the surface under test, near its focus. The observer is behind the ruling, as Fig. 3 shows, with the light entering the eye. The dark bands in the ruling intercept light, forming shadows on the illuminated optical surface. These shadows will be straight and parallel only if the reflected wavefront is perfectly spherical. Otherwise, the fringes will be curves whose shape and separation depends on the wavefront deformations. The Ronchi test

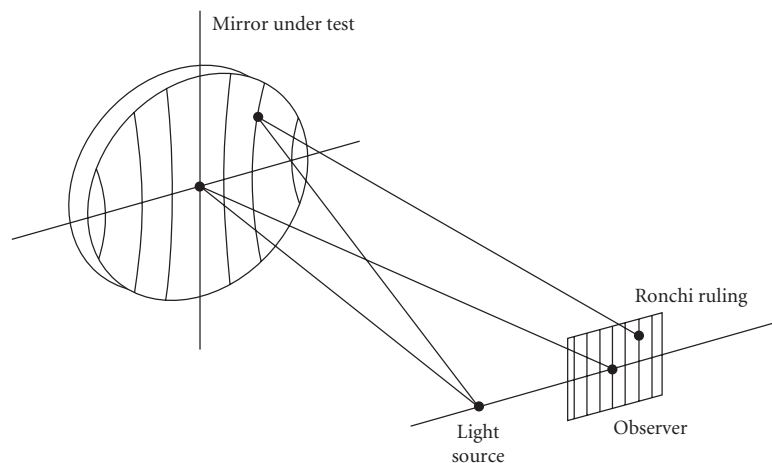


FIGURE 3 Testing a concave surface by means of the Ronchi test.

measures the transverse aberrations in the direction perpendicular to the slits on the grating. The wavefront deformations $W(x, y)$ are related to the transverse aberrations $TA_x(x, y)$ and $TA_y(x, y)$ by the following well-known relations:

$$TA_x(x, y) = -r \frac{\partial W(x, y)}{\partial x} \quad (1)$$

and

$$TA_y(x, y) = -r \frac{\partial W(x, y)}{\partial y} \quad (2)$$

where r is the radius of curvature of the wavefront $W(x, y)$. Thus, if we assume a ruling with period d , the expression describing the m th fringe on the optical surface is given by

$$\frac{\partial W(x, y)}{\partial x} = -\frac{md}{r} \quad (3)$$

Each type of aberration wavefront has a characteristic Ronchi pattern, as shown in Fig. 4; thus, the aberrations in the optical system may be easily identified, and their magnitude estimated. We may interpret the Ronchi fringes not only as geometrical shadows, but also as interferometric fringes, identical with those produced by a lateral shear interferometer.

Hartmann Test

J. Hartmann⁵ invented his test in Germany. It is one of the most powerful methods to determine the figure of a concave spherical or aspherical mirror. Figure 5 shows the optical configuration used

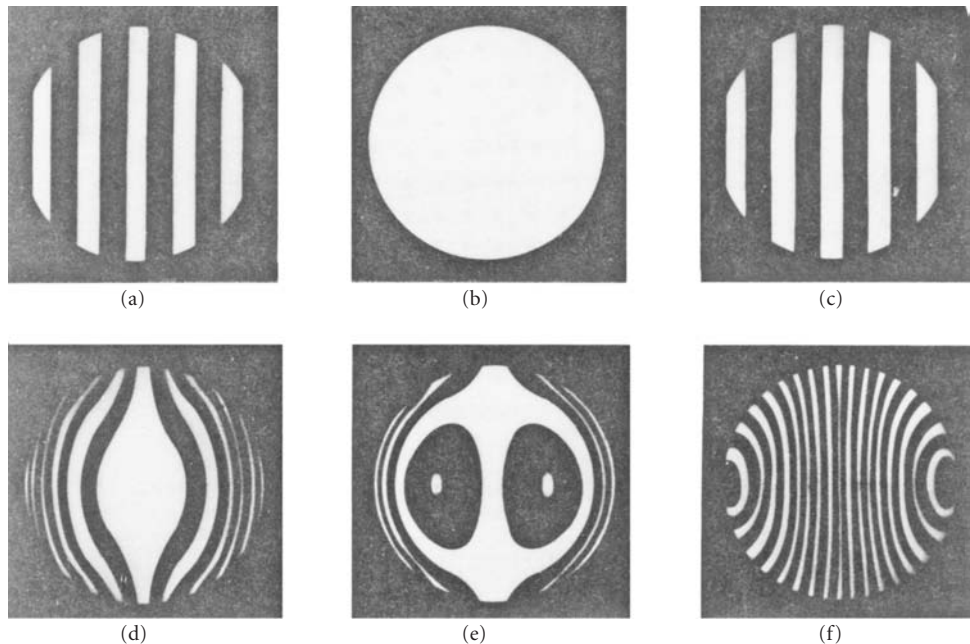


FIGURE 4 Typical Ronchi patterns for a spherical and a parabolic mirror for different positions of the Ronchi ruling.

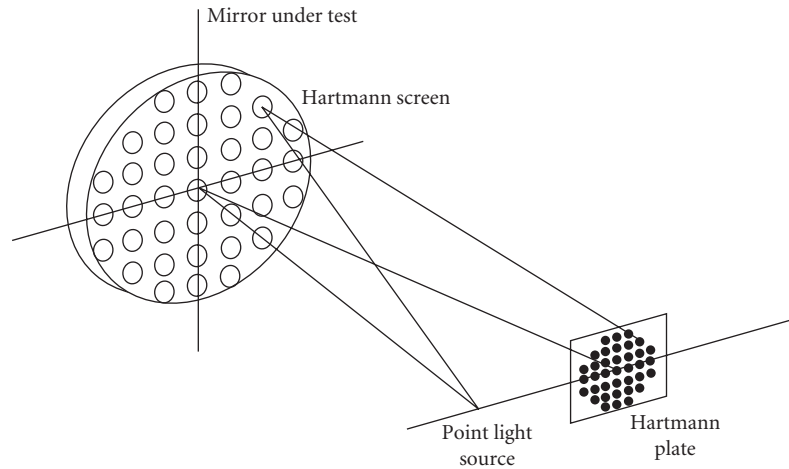


FIGURE 5 Optical arrangement to perform the Hartmann test.

in this test, where a point light source illuminates the optical surface, with its Hartmann screen in front of it. The light beams reflected through each hole on the screen are intercepted on a photographic plate near the focus. Then, the position of the recorded spots is measured to find the value of the transverse aberration on each point. If the screen has a rectangular array of holes, the typical Hartmann plate image for a parabolic mirror looks like that in Fig. 6. The wavefront $W(x, y)$ may be obtained from integration of Eqs. (1) and (2) as follows:

$$W(x, y) = -\frac{1}{r} \int_0^x TA_x(x, y) dx \quad (4)$$

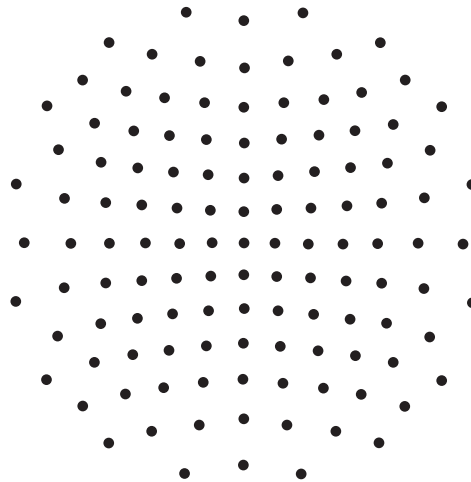


FIGURE 6 Array of spots in a Hartmann plate of a parabolic mirror.

and

$$W(x, y) = -\frac{1}{r} \int_0^y TA_y(x, y) dy \quad (5)$$

After numerical integration of the values of the transverse aberrations, this test provides the concave surface shape with very high accuracy. If the surface is not spherical, the transverse aberrations to be integrated are the difference between the measured values and the ideal values for a perfect surface. Extended, localized errors, as well as asymmetric errors like astigmatism, are detected with this test. The two main problems of this test are that small, localized defects are not detected if they are not covered by the holes on the screen. Not only is this information lost, but the integration results will be false if the localized errors are large. The second important problem of the Hartmann test is that it is very time consuming, due to the time used in measuring all the data points on the Hartmann plate. These problems are avoided by complementing this test with the Foucault test, using an Offner compensator, in order to be sure about the smoothness of the surface (discussed under “Measuring Aspherical Wavefronts”). Various stratagems are available to speed the process. These include modulating the light at different frequencies at each of the holes. Variations also include measuring in front of, behind, or at the focus to get slope information. This technique can be considered an experimental ray trace.

Hartmann-Shack Test

Platt and Shack,⁶ proposed using a lenticular screen, instead of a screen with an array of holes, as illustrated in Fig. 7. This is a simple but important modification from the classic Hartmann. Some differences are

- (a) In the Hartmann test the pattern is obtained in focused convergent light beam, near the focus. On the other hand, in the Hartmann-Shack the test is made in a nearly collimated beam of light.
- (b) A practical advantage of the Hartmann-Shack method is that any positive or negative power can be easily detected and measured.

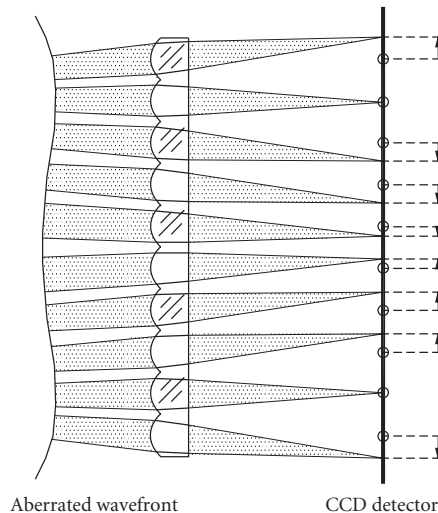


FIGURE 7 Hartmann-Shack Test.

- (c) A second advantage is that each of the spots is individually focused on the detector, making the light energy density of the spot higher than in the Hartmann test.
- (d) The Hartmann-Shack lenticular screen can be made with two identical layers of cylindrical lenses perpendicular to each other, or with a lenslet arrays in molded plastic, glass, or fused silica.

If the wavefront is flat, the light beam passing through each lens is focused close to the optical axis of each lenslet. Since the lens array is not perfect, the lenticular array must be previously calibrated with a reference well-known flat wavefront.

The spot displacement on the detector is equal to the wavefront slope multiplied by the focal length of the lenslet, thus, a shorter focal length will give a greater dynamic range but a reduced angular sensitivity. The optimum focal length depends on the application.

13.4 INTERFEROMETRIC TESTS

Classical geometrical tests are very simple, but they do not provide the accuracy of the interferometric tests. Quite generally, an interferometric test produces an interferogram by producing the interference between two wavefronts. One of these two wavefronts is the wavefront under test. The other wavefront is either a perfectly spherical or flat wavefront, or a copy of the wavefront under test.

When the second wavefront is perfectly spherical or flat, this wavefront acts as a reference. The separation between the two wavefronts, or optical path difference $OPD(x, y)$, is a direct indication of the deformations $W(x, y)$ of the wavefront under test. Then, we may simply write $W(x, y) = OPD(x, y)$. There are many types of interferometers producing interferograms of these type of interferograms, for example, the Twyman-Green and the Fizeau interferometers. Some other interferometers can be considered as modifications of these two basic interferometers, such as the Point Diffraction and the Burch interferometers, and many others that will not be described.

Twyman-Green Interferometer

The Twyman-Green interferometer is illustrated in Fig. 8. The light from a monochromatic point light source is collimated to produce a flat wavefront. Then, the two interfering wavefronts are generated by means of a partially reflective and partially transmitting glass plate, called beam splitter.

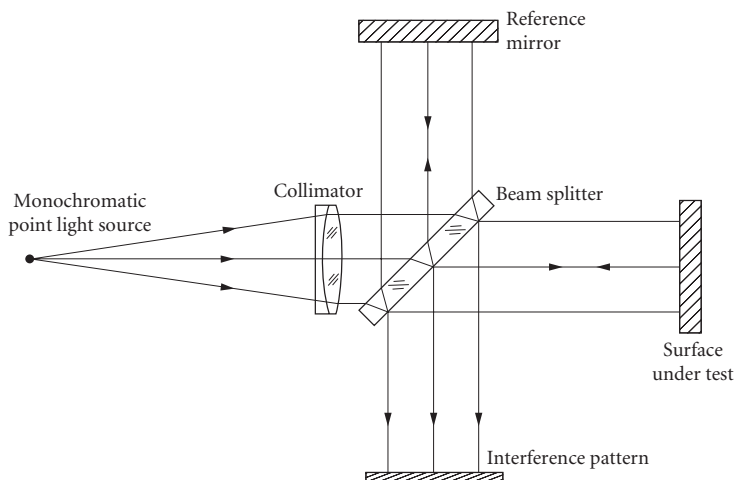


FIGURE 8 Twyman-Green interferometer.

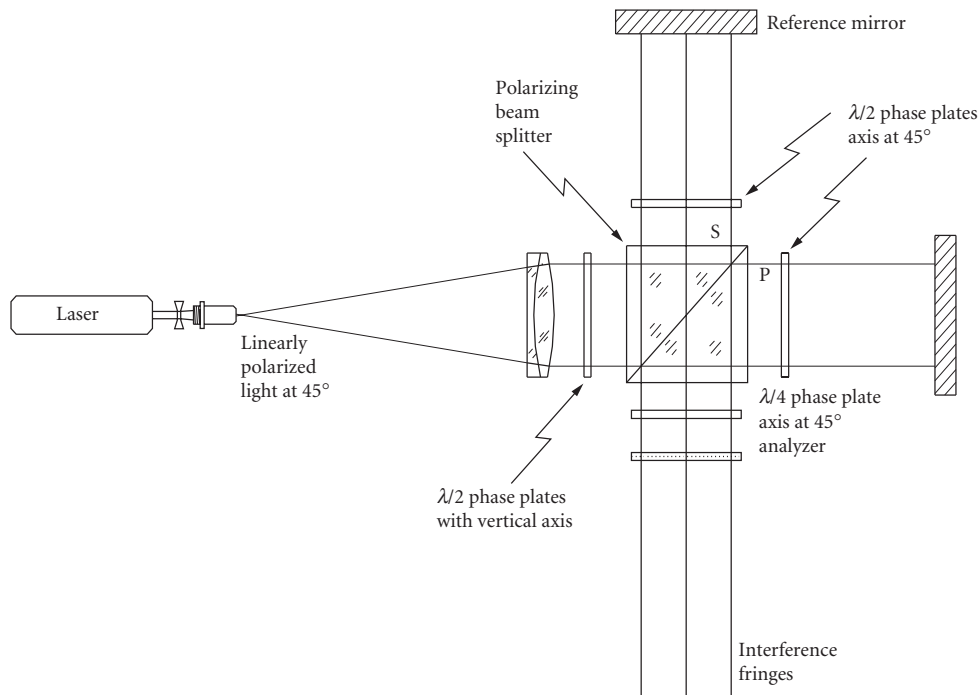


FIGURE 9 Twyman-Green interferometer with polarized beam splitter.

After the beam splitter two flat wavefronts travel in orthogonal directions, one of them to the flat reference mirror and the other to the surface or optical element under test. After returning to the beam splitter, the two wavefronts are recombined to produce an interference pattern. The beam splitter can be oriented at 45° as in Fig. 8, but sometimes a different angle is chosen, for example, a Brewster angle to avoid the reflected beam from the second face on the beam splitter.

Instead of a plane parallel beam splitter, sometimes a polarizing cube beam splitter is used, as in Fig. 9. In this system the plane wavefront entering the beam splitter is linearly polarized at an angle of 45° with respect to the plane of the interferometer. Then, the two wavefronts exiting the cube in orthogonal directions will also be linearly polarized but one of them in the vertical plane and the other in the horizontal plane. A $\lambda/4$ phase plate is located at each of the two exiting faces on the cube. These phase plates produce circularly polarized beams, one going to the reference mirror and the other to the surface under test, but one is right handed and the other is left handed. When arriving back to the cube, after passing twice through the phase plates, the two beams will be again linearly polarized, one in the vertical plane and the other in the horizontal plane. However, these planes of polarization will be orthogonal to the planes of polarization when the wavefront exited the cube. Thus, the two wavefronts are sent to the observation plane and not back to the light source.

Two important facts should be noticed: (a) that the two wavefronts are orthogonally polarized and hence they can not interfere and (b) that there are not any light beams going back to the light source to produce a complementary pattern as in the classic Twyman-Green interferometer. In order to produce observable fringes a linear polarizer should be placed just before the observing plane.

This interferometer with a polarizing beam splitter has many practical advantages.

Fizeau Interferometer

A Fizeau interferometer, illustrated in Fig. 10, is also a two-beam system like the Twyman-Green interferometer. The main difference is that the plate beam splitter is not at 45° with the illuminated

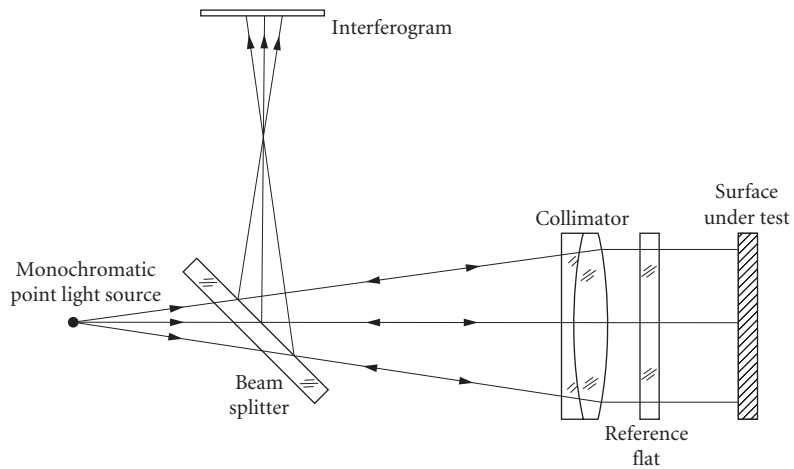


FIGURE 10 Fizeau interferometer.

collimated beam, but perpendicular to its incidence path. Some important practical advantages are that (a) the beam splitter can be smaller for the same aperture, (b) it is more compact, and (c) it is easier to align.

Figure 11 shows some typical interferograms for the Seidel primary aberrations obtained with a Twyman-Green or a Fizeau interferometer.¹ The mathematical analysis of interferograms for wavefronts with arbitrary deformations is a research topic of great interest that has been described in a large number of publications.⁷

Common Path Interferometer

A common path interferometer is one for which the two interfering beams travel the same paths. The optical path difference at the center of the optical axis is zero and cannot be modified. Thus interference with a white light source can be easily achieved. An example of this kind of interferometer is the point-diffraction interferometer first described by Linnik in 1933 and later rediscovered by Smart and Strong.⁸ The lens of optical element under test focuses the light at the center of a small diffracting plate as illustrated in Fig. 12. This diffracting plate is coated with a thin partially transmitting film with a small uncoated disk at its center. The diameter of the central clear disk is about the size of the diffraction air disk produced by a perfect optical system. If the wavefront from the system is not spherical but distorted, the focused spot would be larger than the central disk. Then, two wavefronts are produced. One is a reference spherical wavefront arising from the light diffracted at the central disk. The undiffracted light passing outside of the disk is the wavefront under test.

The fringe patterns in the point diffraction interferometer are identical to those produced by the Twyman-Green interferometer.

Lateral Shearing Interferometers

When the second wavefront is not perfectly flat or spherical, but a copy of the wavefront under test, its relative dimensions or orientation must be changed (sheared) in some way with respect to the wavefront under test. Otherwise, no information about the wavefront deformations is obtained, because the fringes will always be straight and parallel independent of any aberrations. There are several kinds of shearing interferometers, depending on the kind of transformation applied to the reference wavefront.

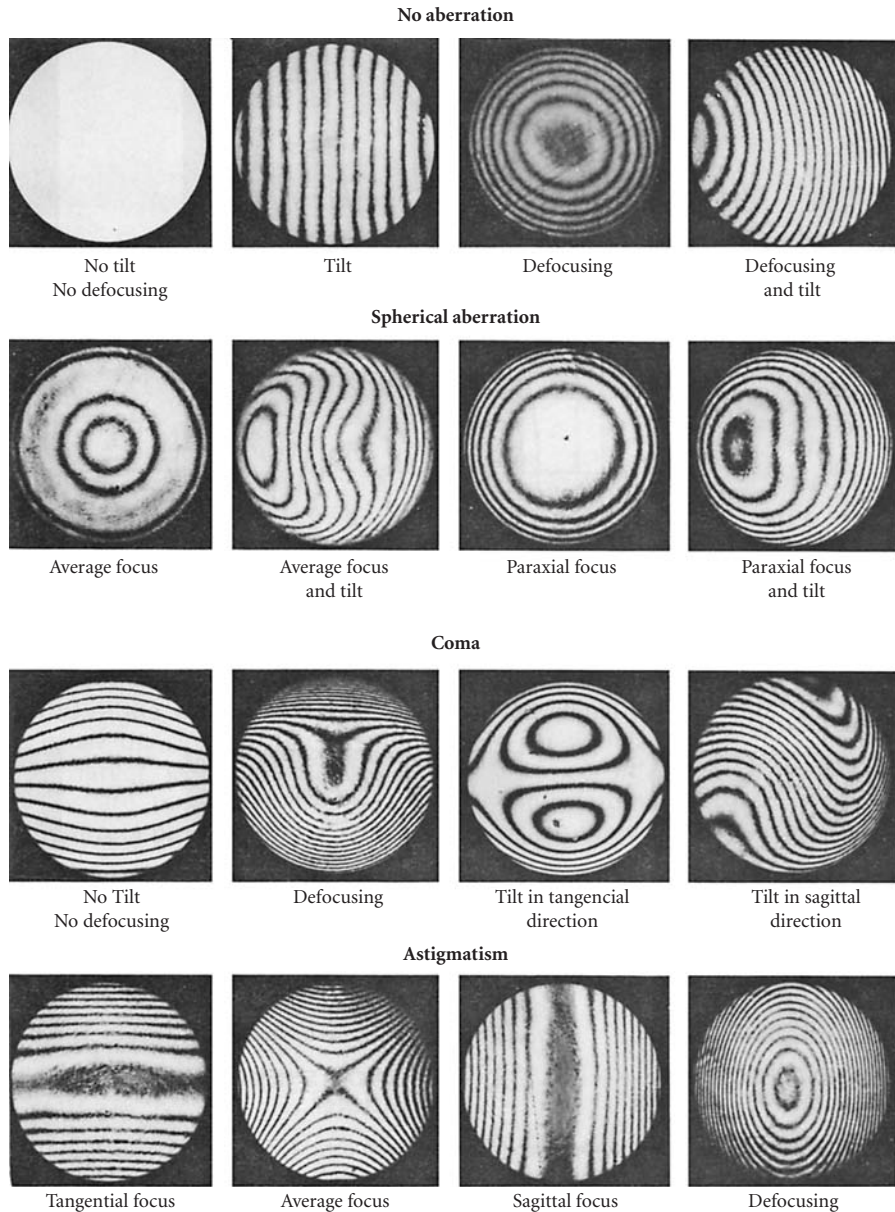


FIGURE 11 Twyman-Green interferograms. (From Malacara.¹)

The most popular of these instruments is the lateral shearing interferometer, with the reference wavefront laterally displaced with respect to the other, as in the interferograms in Fig. 13 shows. The optical path difference $OPD(x, y)$ and the wavefront deformations $W(x, y)$ are related by

$$OPD(x, y) = W(x, y) - W(x - S, y) \quad (6)$$

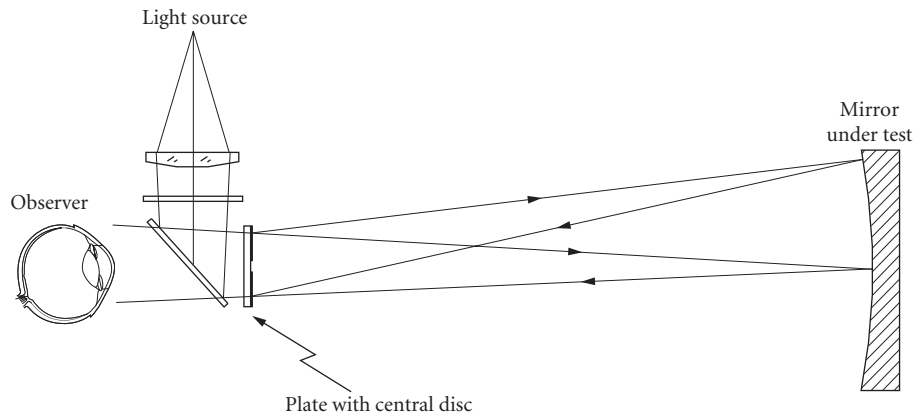


FIGURE 12 Point diffraction interferometer.

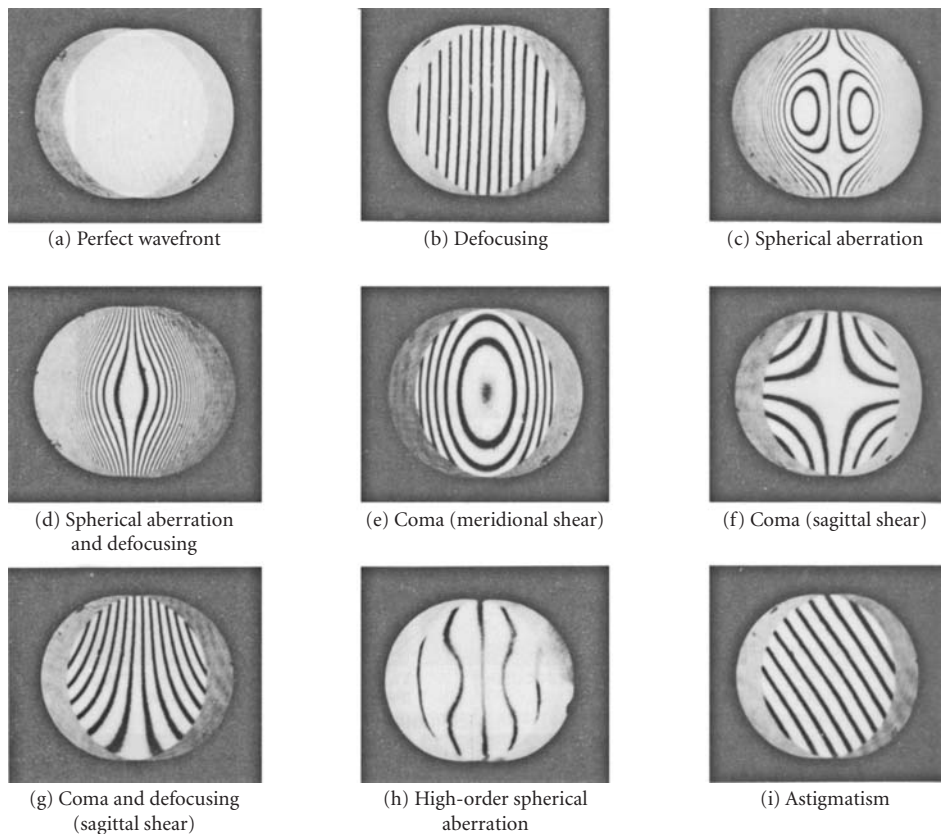


FIGURE 13 Laterally sheared interferograms. (From Malacara.¹)

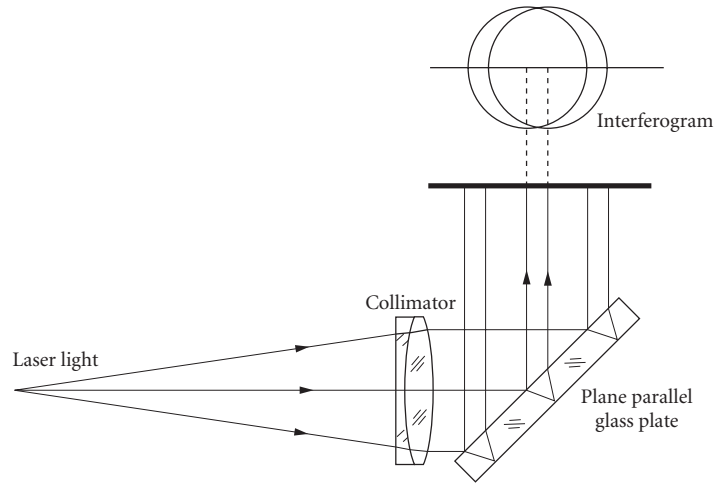


FIGURE 14 Murty's lateral shear interferometer.

where S is the lateral shear of one wavefront with respect to the other. If the shear is small with respect to the diameter of the wavefront, this expression may be approximated by

$$\text{OPD}(x, y) = -S \frac{\partial W(x, y)}{\partial x} = -\frac{S}{r} TAx(x, y) \quad (7)$$

This relation suggests that the parameter being directly measured is the slope in the x direction of the wavefront (x component TAx of the transverse aberration). An example of a lateral shear interferometer is the Murty interferometer, illustrated in Fig. 14.

Radial, Rotational, and Reversal Shearing Interferometers

There are also radial, rotational, and reversal shearing interferometers, where the interfering wavefronts are as illustrated in Fig. 15. A radial shear interferometer with a large shear approaches an interferometer with a perfect reference wavefront. These interferometers produce fringe patterns by the interference of two wavefronts with the same aberrations and deformations. The difference between the two interfering wavefronts is their size or orientation.

The optical path in the radial shear interferometer can be represented by

$$\text{OPD}(x, y) = W(x, y) - W(\rho x, \rho y) \quad (8)$$

A typical radial shear interferogram is in Fig. 16.

In the rotational shear interferometer. The two interfering wavefronts have the same size, but one of those is rotated with respect to the other. In the particular case on a 180° rotation the sensitivity of the interferometer is zero for symmetrical (even) aberrations, like spherical aberration. However, the sensitivity is doubled for antisymmetrical (odd) aberrations, like coma.

In a reversing shear interferometer one of the two wavefronts is reversed with respect to the other about any diameter on the wavefront's pupil. As in the rotational shear interferometer, the sensitivity to aberrations is symmetric with respect to the axis of reversion. Also, the sensitivity to aberration antisymmetric about the axis of reversion is doubled.

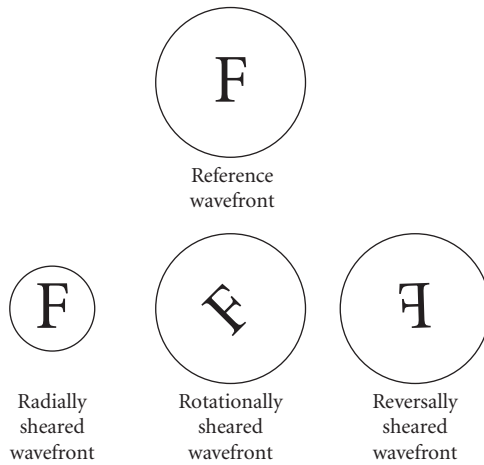


FIGURE 15 Wavefronts in radial, rotational, and reversal shear interferometers.

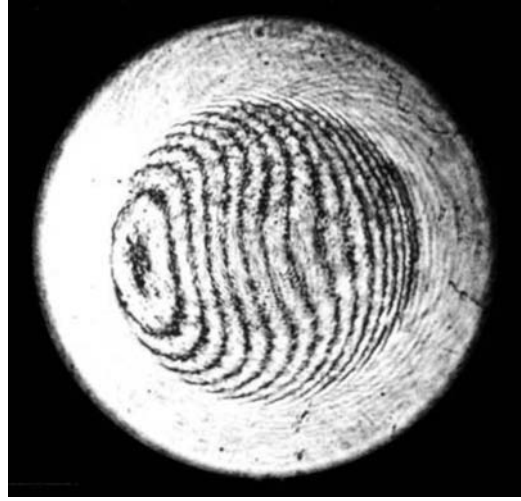


FIGURE 16 A radial shear interferogram.

13.5 INCREASING THE SENSITIVITY OF INTERFEROMETERS

The sensitivity of interferometers is a small fraction of the wavelength being used (about $\lambda/20$). There are several methods to increase this sensitivity, but the most common methods will now be described.

Multiple-Reflection Interferometers

A method to increase the sensitivity of interferometric methods is to use multiple reflections, as in the Fabry-Perot interferometer. The Newton as well as the Fizeau interferometers can be made multiple-reflection interferometers by coating the reference surface and the surface under test with a high-reflection film. Then, the fringes are greatly narrowed and their deviations from straightness are more accurately measured.⁹

Multiple-Pass Interferometers

Another method to increase the sensitivity of interferometers is by double, or even multiple, pass. An additional advantage of double-pass interferometry is that the symmetrical and antisymmetrical parts of the wavefront aberration may be separated. This makes their identification easier, as Hariharan and Sen¹⁰ have proved. Several arrangements have been devised to use multiple pass.¹¹

Zernike Tests

The Zernike phase-contrast method is another way to improve the sensitivity of an interferometer to small aberrations. It was suggested by Zernike as a way to improve the knife-edge test.¹² There are several versions of this test. The basic principle in all of them is the introduction of a

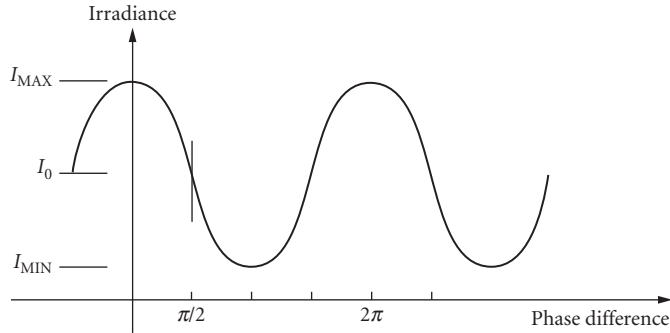


FIGURE 17 Irradiance in an interference pattern, as a function of the phase difference between the two interfering waves.

phase difference equal to $\lambda/2$ between the wavefront under test and the reference wavefront. To understand why this phase difference is convenient, let us consider two interfering beams and irradiances $I_1(x, y)$ and $I_2(x, y)$ and a phase $\phi(x, y)$ between them. The final irradiance $I(x, y)$ in the interferogram is given by

$$I(x, y) = I_1(x, y) + I_2(x, y) + 2\sqrt{I_1(x, y)I_2(x, y)}\cos\phi(x, y) \quad (9)$$

Thus, the irradiance $I(x, y)$ of the combination would be a sinusoidal function of the phase, as illustrated in Fig. 17. If the phase difference is zero for a perfect wavefront, deformations of the wavefront smaller than the wavelength of the light will not be easy to detect, because the slope of the function is zero for a phase near zero. The slope of this function is larger and linear for a phase value of 90° . Thus, the small wavefront deformations are more easily detected if the interferometer is adjusted, so that the wavefronts have a phase difference equal to 90° when the wavefront under test is perfect.

13.6 INTERFEROGRAM EVALUATION

An interferogram may be analyzed in several manners. One way begins by measuring several points on the interferogram, on top of the fringes. Then, the wavefront values between the fringes are interpolated. Another way uses a Fourier analysis of the interferogram. A third method interprets the fringe deformations as a phase modulation.

Fixed Interferogram Evaluation

Once the interferogram has been formed, a quantitative evaluation of it is a convenient method to find the wavefront deformations. The fixed interferogram evaluation by fringe measurements is done by measuring the position of several data points located on top of the fringes. These measurements are made in many ways, for example, with a measuring microscope, with a digitizing tablet, or with a video camera connected to a computer.

The fringe centers can be located either manually, using a digitizing tablet, or automatically, with the computer directly examining a single fringe image that has been captured using a digital frame grabber. After locating the fringe centers, fringe order numbers must be assigned to each point. The wavefront can then be characterized by direct analysis of the fringe centers. If desired, instead of global interpolation, a local interpolation procedure may be used.

To analyze the fringes by a computer, they must first be digitized by locating the fringe centers, and assigning fringe order numbers to them. The optical path difference (OPD) at the center of any fringe is a multiple m of the wavelength ($OPD = m\lambda$), where m is the fringe order. To obtain the

wavefront deformation, only the relative values of the fringe order are important. So any value of the fringe order may be assigned to the first fringe being measured. However, for the second fringe, it may be increased or decreased by one. This choice affects only the sign of the OPD. An important disadvantage of the fixed interferogram analysis is that the sign of the OPD cannot be obtained from the interferogram alone. This information can be retrieved if the sign of any term in the wavefront deformation expression, like defocusing or tilt, is previously determined when taking the interferogram.

Fringes have been digitized using scanners,¹³ television cameras,¹⁴ photoelectric scanners, and digitizing tablets. Review articles by Reid^{15,16} give useful references for fringe digitization using television cameras.

Global and Local Interpolation of Interferograms

After the measurements are made, the wavefront is computed with the measured points. The data density depends on the density of fringes in the interferogram. Given a wavefront deformation, the ratio of the fringe deviations from straightness to the separation between the fringes remains a constant, independently of the number of fringes introduced by tilting of the reference wavefront. If the number of fringes is large due to a large tilt, the fringes look more straight than if the number of fringes is small. Thus, the fringe deviations may more accurately be measured if there are few fringes in the interferogram. Thus, information about many large zones is lost. A way to overcome this problem is to interpolate intermediate values by any of several existing methods. One method is to fit the wavefront data to a two-dimensional polynomial with a least-squares fitting, as described by Malacara et al.¹⁷ or by using splines as described by Hayslett and Swantner¹⁸ and Becker et al.¹⁹ Unfortunately, this procedure has many problems if the wavefront is very irregular. The values obtained with the polynomial may be wrong, especially near the edge, or between fringes if the wavefront is too irregular.

The main disadvantage of global fits is that they smooth the measured surface more than desired. Depending on the degree of the polynomial, there will only be a few degrees of freedom to fit many data points. It is even possible that the fitted surface will pass through none of the measured points. If the surface contains irregular features that are not well described by the chosen polynomial, such as steps or small bumps, the polynomial fit will smooth these features. Then, they will not be visible in the fitted surface.

Global interpolation is done by least-squares fitting the measured data to a two-dimensional polynomial in polar coordinates. The procedure to make the least-squares fitting begins by defining the variance of the discrete wavefront fitting as follows:

$$\sigma = \frac{1}{N} \sum_{i=1}^N [W_i' - W(\rho_i, \theta_i)]^2 \quad (10)$$

where N is the number of data points, W_i is the measured wavefront deviation for data point i , and $W(i, \theta_i)$ is the functional wavefront deviation after the polynomial fitting. The only requirement is that this variance or fit error is minimized. It is well known that the normal least-squares procedure leads to the inversion of an almost singular matrix. Then, the round-off errors will be so large that the results will be useless. To avoid this problem, the normal approach is to fit the measured points to a linear combination of polynomials that are orthogonal over the discrete set of data points. Thus, the wavefront is represented by

$$W(\rho_i, \theta_i) = \sum_{n=1}^L B_n V_n(\rho_i, \theta_i) \quad (11)$$

$V(\rho, \theta)$ are polynomials of degree r and not the monomials x . These polynomials satisfy the orthogonality condition

$$\sum_{i=1}^N V_n(\rho_i, \theta_i) V_m(\rho_i, \theta_i) = F_n \rho_{nm} \quad (12)$$

where $F_n = \sum V_n^2$.

The advantage of using these orthogonal polynomials is that the matrix of the system becomes diagonal and there is no need to invert it.

The only problem that remains is to obtain the orthogonal polynomials by means of the Gram-Schmidt orthogonalization procedure. It is important to notice that the set of orthogonal polynomials is different for every set of data points. If only one data point is removed or added, the orthogonal polynomials are modified. If the number of data points tends to infinity and they are uniformly distributed over a circular pupil with unit radius, these polynomials $V_r(\rho, \theta)$ approach the Zernike polynomials.²⁰

Several properties of orthogonal polynomials make them ideal for representing wavefronts, but the most important of them is that we may add or subtract one or more polynomial terms without affecting the fit coefficients of the other terms. Thus, we can subtract one or more fitted terms—defocus, for example—without having to recalculate the least-squares fit. In an interferometric optical testing procedure the main objective is to determine the shape of the wavefront measured with respect to a best-fit sphere. Nearly always it will be necessary to add or subtract some terms.

The only problem with these orthogonal polynomials over the discrete set of data points is that they are different for every set of data points. A better choice for the wavefront representation is the set of Zernike polynomials, which are orthogonal on the circle with unit radius, as follows:

$$\int_0^1 \int_0^{2\pi} U_n(\rho, \theta) U_m(\rho, \theta) \rho d\rho d\theta = F_{nm} \delta_{nm} \quad (13)$$

These polynomials are not exactly orthogonal on the set of data points, but they are close to satisfying this condition. Therefore, it is common to transform the wavefront representation in terms of the polynomials V_n to another similar representation in terms of Zernike polynomials $U_n(\rho, \theta)$, as

$$W(\rho, \theta) = \sum_{n=1}^L A_n U_n(\rho, \theta) \quad (14)$$

Fourier Analysis of Interferograms

A completely different way to analyze an interferogram without having to make any interpolation between the fringes is by a Fourier analysis of the interferogram. An interpolation procedure is not needed because the irradiance at a fine two-dimensional array of points is measured and not only at the top of the fringes. The irradiance should be measured directly on the interferogram with a two-dimensional detector or television camera, and not on a photographic picture. Womack,²¹ Macy,²² Takeda et al.,²³ and Roddier and Roddier²⁴ have studied in detail the Fourier analysis of interferograms to obtain the wavefront deformations.

Consider an interferogram produced by the interference of the wavefront under test and a flat reference wavefront, with a large tilt between them, as in the interferogram in Fig. 18. The tilt is about the y axis, increasing the distance between the wavefronts in the x direction. The picture of this interferogram may be thought of as a hologram reconstructing the wavefront. Thus, three wavefronts (images) are generated when this hologram is illuminated with a flat wavefront. In order to have complete separation between these images, the tilt between the wavefronts must be large enough, so that the angle between them is not zero at any point over the interferogram. This is equivalent to saying that the fringes must be open, and never cross any line parallel to the x axis more than once. One image is the wavefront under test and another is the conjugate of this wavefront.

If the tilt between the wavefront is θ and the wavefront shape is $W(x, y)$, the irradiance is given by

$$I(x, y) = I_1(x, y) + I_2(x, y) + 2\sqrt{I_1(x, y)I_2(x, y)}\cos(\phi_0 + kx\sin\theta + kW(x, y)) \quad (15)$$

where $k = 2\pi/\lambda$. This expression may be rewritten as

$$I = [I_1 + I_2] + \sqrt{I_1 I_2} e^{i(kx\sin\theta + kW)} + \sqrt{I_1 I_2} e^{-i(kx\sin\theta + kW)} \quad (16)$$

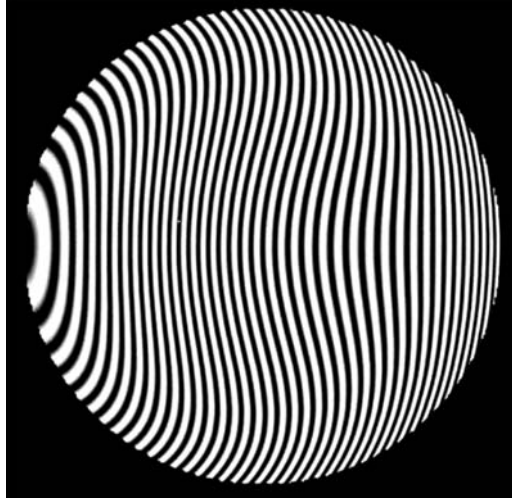


FIGURE 18 Interferogram with a large tilt (linear carrier) to avoid closed fringes.

The first term represents the zero order, the second is the real image, and the third is the virtual image. We also may say that the Fourier transform of the interferogram is formed by a Dirac impulse $\delta(f)$ at the origin and two terms shifted from the origin, at frequencies $+f_0$ and $-f_0$. The quantity f is the spatial frequency, defined by the tilt between the reference wavefront and the wavefront under test ($f = \sin \theta / \lambda$). These terms may be found by taking the Fourier transform of the interferogram. The term at f_0 is due to the wavefront under test. This wavefront may be obtained by taking the Fourier transform of this term, mathematically isolated from the others. This method is performed in a computer by using the fast Fourier transform. The undesired terms are simply eliminated before taking the second fast Fourier transform in order to obtain the wavefront.

Direct Interferometry

This is another method to obtain the wavefront from an interferogram without the need of any interpolation. As in the Fourier method, the image of the interferogram is directly measured with a two-dimensional detector or television camera. The interferogram must have many fringes, produced with a large tilt between the wavefronts. The requirements for the magnitude of this tilt are the same as in the Fourier method.

Consider the irradiance in the interferogram in Fig. 18 along a line parallel to the x axis. This irradiance plotted versus the coordinate x is a perfectly sinusoidal function only if the wavefront is perfect, that is, if the fringes are straight, parallel, and equidistant. Otherwise, this function appears as a wave with a phase modulation. The phase-modulating function is the wavefront shape $W(x, y)$. If the tilt between the wavefronts is θ , the irradiance function is described by Eq. (15). If ϕ_0 is a multiple of 2π , this expression may be rewritten as

$$I(x, y) = I_1 + I_2 + 2\sqrt{I_1 I_2} \cos(kx \sin \theta + kW) \quad (17)$$

Multiplying this phase-modulated function by a sinusoidal signal with the same frequency as the carrier $\sin(kx \sin \theta)$ a new signal S is obtained. Similarly, multiplying by a cosinusoidal signal

$\cos(kx \sin \theta)$ a new signal C is obtained. If all terms in the signals S and C with frequencies equal to or greater than the carrier frequency are removed with a low-pass filter, they become

$$S(x, y) = -\sqrt{I_1 I_2} \sin kW(x, y) \quad (18)$$

$$C(x, y) = \sqrt{I_1 I_2} \cos kW(x, y) \quad (19)$$

then, the wavefront $W(x, y)$ is given by

$$W(x, y) = -\frac{1}{k} \tan^{-1} \left[\frac{S(x, y)}{C(x, y)} \right] \quad (20)$$

which is our desired result.

13.7 PHASE-SHIFTING INTERFEROMETRY

All the methods just described are based on the analysis of a single static interferogram. Static fringe analysis is generally less precise than phase-shifting interferometry, by more than one order of magnitude. However, fringe analysis has the advantage that a single image of the fringes is needed. On the other hand, phase-shifting interferometry requires several images, acquired over a long time span during which the fringes must be stable. This is the main reason why phase-shifting interferometry has seldom been used for the testing of astronomical optics.

Phase-shifting interferometry^{25,26} is possible, thanks to modern tools like array detectors and microprocessors. Figure 19 shows a Twyman-Green interferometer adapted to perform phase-shifting interferometry. Most conventional interferometers, like the Fizeau and the Twyman-Green, have been used to do phase shifting. A good review about these techniques may be found in the review article by Creath.²⁷

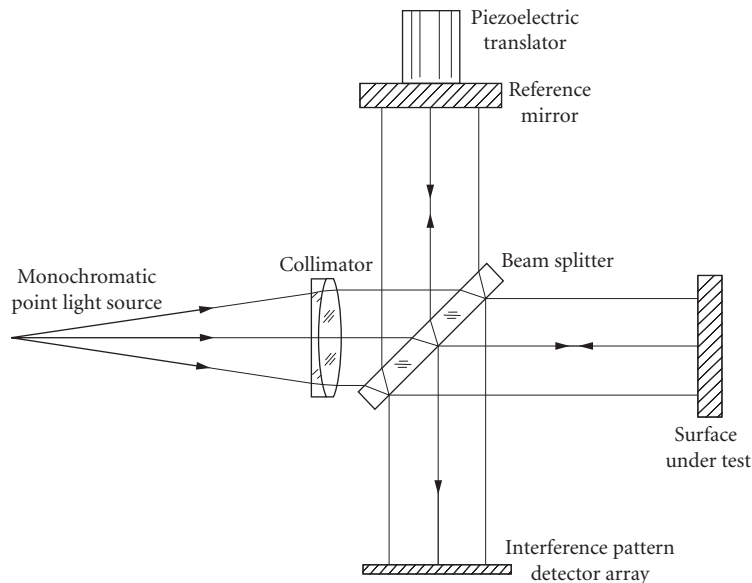


FIGURE 19 Twyman-Green interferogram adapted to do phase shifting.

In phase-shifting interferometers, the reference wavefront is moved along the direction of propagation, with respect to the wavefront under test, changing in this manner their phase difference. This phase shifting is made in steps or in a continuous manner. Of course, this relative displacement of one wavefront with respect to the other may only be achieved through a momentary or continuous change in the frequency of one of the beams, for example, by Doppler shift, moving one of the mirrors in the interferometer. In other words, this change in the phase is accomplished when the frequency of one of the beams is modified in order to form beats.

By measuring the irradiance changes for different values of the phase shifts, it is possible to determine the initial difference in phase between the wavefront under test and the reference wavefront, for that measured point over the wavefront. By obtaining this initial phase difference for many points over the wavefront, the complete wavefront shape is thus determined. If we consider any fixed point in the interferogram, the initial phase difference between the two wavefronts has to be changed in order to make several measurements.

One method that can be used to shift this phase is by moving the mirror for the reference beam along the light trajectory, as in Fig. 19. This can be done in many ways, for example, with a piezoelectric crystal or with a coil in a magnetic field. If the mirror moves with a speed V , the frequency of the reflected light is shifted by an amount equal to $\Delta\nu = 2V/\lambda$.

Another method to shift the phase is by inserting a plane parallel glass plate in the light beam (see Fig. 20). Then the plate is rotated about an axis perpendicular to the optical axis. The phase may also be shifted by means of the device shown in Fig. 21. The first quarter-wave retarding plate is stationary, with its slow axis at 45° with respect to the plane of polarization of the incident linearly polarized light. This plate also transforms the returning circularly polarized light back to linearly

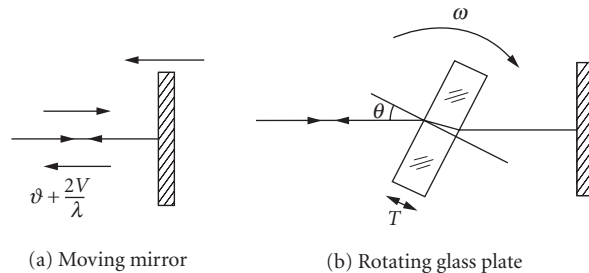


FIGURE 20 Obtaining the phase shift by means of a moving mirror or a rotating glass plate.

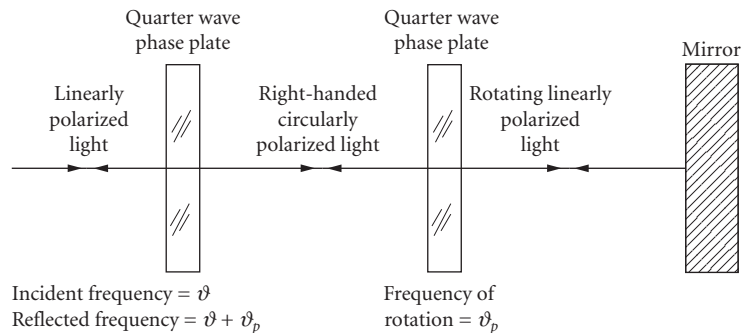


FIGURE 21 Obtaining the phase shift by means of phase plates and polarized light, with a double pass of the light beam.

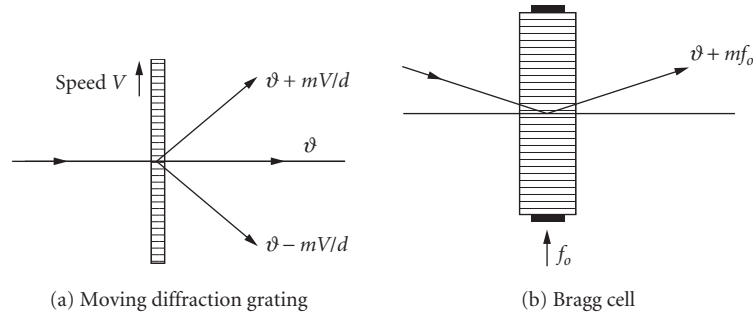


FIGURE 22 Obtaining the phase shift by means of diffraction: (a) with a diffraction grating and (b) with an acousto-optic Bragg cell.

polarized. The second phase retarder is also a quarter-wave plate, it is rotating, and the light goes through it twice; therefore, it is acting as a half-wave plate.

Still another manner to obtain the shift of the phase is by a diffraction grating moving perpendicularly to the light beam, as shown in Fig. 22a, or with an acousto-optic Bragg cell, as shown in Fig. 22b. The change in the frequency is equal to the frequency f of the ultrasonic wave times the order of diffraction m . Thus: $\Delta\nu = mf$.

The nonshifted relative phase of the two interfering wavefronts is found by measuring the irradiance with several predefined and known phase shifts. Let us assume that the irradiance of each of the two interfering light beams at the point x, y in the interference patterns are $I_1(x, y)$ and $I_2(x, y)$ and that their phase difference is $\phi(x, y)$. It was shown before, in Eq. (9), that the resultant irradiance $I(x, y)$ is a sinusoidal function describing the phase difference between the two waves. The basic problem is to determine the nonshifted phase difference between the two waves, with the highest possible precision. This may be done by any of several different procedures.

Phase-Stepping and Four Steps Algorithms

This method²⁷ consists of measuring the irradiance values for several known increments of the phase. There are several versions of this method, which will be described later. The measurement of the irradiance for any given phase takes some time, since there is a time response for the detector. Therefore, the phase has to be stationary during a short time in order to take the measurement. Between two consecutive measurements, the phase is changed by an increment α_i . For those values of the phase, the irradiance becomes

$$I(x, y) = I_1 + I_2 + 2\sqrt{I_1 I_2} \cos(\phi + \alpha_i) \quad (21)$$

There are many different algorithms, with many different phase steps, as shown in Fig. 23. The minimum number of steps needed to reconstruct this sinusoidal function is three. As an example with four steps,

$$I_A = I_1 + I_2 + 2\sqrt{I_1 I_2} \cos\phi \quad (22)$$

$$I_B = I_1 + I_2 - 2\sqrt{I_1 I_2} \sin\phi \quad (23)$$

$$I_C = I_1 + I_2 - 2\sqrt{I_1 I_2} \cos\phi \quad (24)$$

$$I_D = I_1 + I_2 + 2\sqrt{I_1 I_2} \sin\phi \quad (25)$$

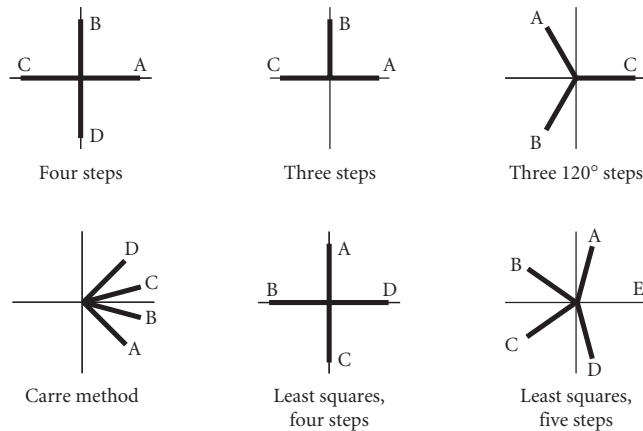


FIGURE 23 Six different ways to shift the phase using phase steps.

Integrating Bucket

In the integrating phase-shifting method the detector continuously measures the irradiance during a fixed time interval, without stopping the phase. Since the phase changes continuously, the average value of the irradiance during the measuring time interval is measured. Thus, the integrating phase-stepping method may be mathematically considered a particular case of the phase-stepping method if the detector has an infinitely short time response. Then, the measurement time interval is reduced to zero. If the measurement is taken, as in Fig. 24, from $\alpha_i + \Delta/2$ to $\alpha_i - \Delta/2$ with center at α_i , then

$$I = \frac{1}{\Delta} \int_{\alpha_i - \Delta/2}^{\alpha_i + \Delta/2} [I_1 + I_2 + 2\sqrt{I_1 I_2} \cos(\phi + \alpha)] d\alpha \quad (26)$$

$$I = I_1 + I_2 + 2\sqrt{I_1 I_2} \text{sinc}(\Delta/2) \cos(\phi + \alpha_i) \quad (27)$$

In general, in the phase-stepping as well as in the integrating phase-shifting methods, the irradiance is measured at several different values of the phase α_i , and then the phase is calculated.

Two Steps Plus One Method

As pointed out before, phase-shifting interferometry is not useful for testing systems with vibrations or turbulence because the three or four interferograms are taken at different times. An attempt

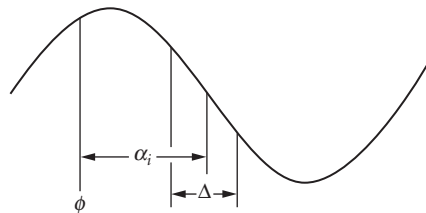


FIGURE 24 Averaged signal measurements with the integrating phase-shifting method.

to reduce this time is the so-called two steps plus one method, in which only two measurements separated by 90° are taken.²⁸ A third reading is taken any time later, of the sum of the irradiance of the beams, independently of their relative phase. This last reading may be taken using an integrating interval $\Delta = 2\pi$. Thus,

$$I_A = I_1 + I_2 + 2\sqrt{I_1 I_2} \cos \phi \quad (28)$$

$$I_B = I_1 + I_2 + 2\sqrt{I_1 I_2} \sin \phi \quad (29)$$

$$I_C = I_1 + I_2 \quad (30)$$

Therefore,

$$\phi = \tan^{-1} \left\{ \frac{I_B - I_C}{I_A - I_C} \right\} \quad (31)$$

Other Phase-Stepping Algorithms

When calculating the phase with several different three or more phase steps, several sources of error affect the accuracy of the result, for example:

- (a) A line miscalibration of the phase shifter. Then the introduced phase steps will have a linear error, which can be interpreted as a change of the reference frequency f_r , making it different from the signed frequency as it should be.
- (b) A nonlinearity in the phase shifter or on the detector that introduces light order harmonics in the detected signal.

These phase errors can be reduced or minimized by properly selecting the number of phase steps and their phase increments. Using Fourier theory as shown by Freischlad and Koliopolus,²⁹ a large number of different algorithms with different contributors and number of phase steps have been described in the literature. Depending on the kind of source error and the maximum number of phase steps desired, the proper algorithm can be selected.

Simultaneous Measurement

It has been said several times that the great disadvantage of phase-shifting interferometry is its great sensitivity to vibrations and atmospheric turbulence. To eliminate this problem, it has been proposed that the different interferograms corresponding to different phases be taken simultaneously.^{30,31} To obtain the phase-shifted interferogram, they have used polarization-based interferometers. The great disadvantage of these interferometers is their complexity. To measure the images these interferometers have to use several television cameras.

Heterodyne Interferometer

When the phase shift is made in a continuous manner rather than in steps, the frequency of the shifting beam is permanently modified, and a beating between the two interferometer beams is formed.³²

The phase of the modulated or beating wave may be determined in many ways. One way is by electronic analog techniques, for example, using leading-edge detectors. Another way is by detecting when the irradiance passes through zero, that is, through the axis of symmetry of the irradiance function.

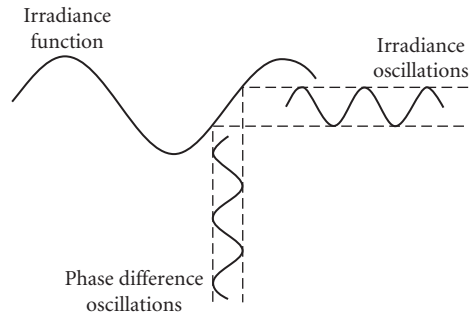


FIGURE 25 Phase-lock method to find the phase with a small sinusoidal modulation of the phase.

Phase Lock

The phase-lock method^{31–35} can be explained with the help of Fig. 25. Assume that an additional phase difference is added to the initial phase $\phi(x, y)$. The additional phase being added has two components: one of them with a fixed value and the other with a sinusoidal time shape. Both components can have any predetermined desired value. Thus, the resultant phase ϕ_r is given by

$$\phi_r = \phi(x, y) + \delta(x, y) + a \sin \omega t \quad (32)$$

then, the irradiance $I(x, y)$ would be given by

$$I = I_1 + I_2 + 2\sqrt{I_1 I_2} \cos[\phi + \delta + a \sin \omega t] \quad (33)$$

The amplitude of the phase oscillations $a \sin t$ is much smaller than π . We may now adjust the fixed phase to a value such that $\phi + \delta = \pi/2 + n\pi$. Then the value of $\cos(\phi + \delta)$ is zero. The curve is antisymmetric at this point; hence, only odd harmonics remain on the irradiance signal. This is done in practice by slowly changing the value of the phase δ , while maintaining the oscillation $a \sin \omega t$, until the maximum amplitude of the first harmonic, or fundamental frequency, is obtained. At this point, then, we have $\delta + \phi = \pi/2 + n\pi$, and since the value of δ is known, the value ϕ has been determined.

13.8 MEASURING ASPHERICAL WAVEFRONTS

The most common type of interferometer, with the exception of lateral or rotational shearing interferometers, produces interference patterns in which the fringes are straight, equidistant, and parallel, when the wavefront under test is perfect and spherical with the same radius of curvature as the reference wavefront.

If the surface under test does not have a perfect shape, the fringes will not be straight and their separations will be variable. The deformations of the wavefront may be determined by a mathematical examination of the shape of the fringes. By introducing a small spherical curvature on the reference wavefront (focus shift) or by changing its angle with respect to the wavefront under test (tilt), the number of fringes in the interferogram may be changed. This is done to reduce the number of fringes as much as possible, since the greater the number of fringes, the smaller the sensitivity of the test. However, for aspherical surfaces this number of fringes cannot be smaller than a certain minimum. The larger the asphericity is, the greater is this minimum number of fringes. Since the fringe

separations are not constant, in some places the fringes will be widely spaced, but in some others the fringes will be too close together.

The sensitivity of the test depends on the separation between the fringes, because an error of one wavelength in the wavefront distorts the fringe shape by an amount equal to the separation between the fringes. Thus, the sensitivity is directly proportional to the fringe separation. When the fringes are widely separated, the sampled points will be quite separated from each other, leaving many zones without any information. On the other hand, where the fringes are very close to each other, there is a high density of sampled data points, but the sensitivity is low.

Then, it is desirable that the spherical aberration of the wavefront under test is compensated in some way, so that the fringes appear straight, parallel, and equidistant, for a perfect wavefront. This is called a null test and may be accomplished by means of some special configurations. These special configurations may be used to conduct a null test of a conic surface. These are described in several books.¹ Almost all of these surfaces have rotational symmetry.

If no testing configuration can be found to get rid of the spherical aberration, additional optical components, called null compensators, have to be used. Many different types of compensators have been invented. The compensators may be refractive (lenses), reflective (mirrors), or diffractive (real or computer-generated holograms).

Refractive or Reflective Compensators

The simplest way to compensate the spherical aberration of a paraboloid or a hyperboloid tested at the center of curvature is a single convergent lens placed near the point of convergence of the rays, as Fig. 26 shows. This lens is called a Dall compensator. Unfortunately, the correction due to a single lens is not complete, so a system of two lenses must be used to obtain a better compensation. This system is called an Offner compensator and is shown in Fig. 27. The field lens L is used to image the surface under test on the plane of the compensating lens L . Mirrors may also be used to design a null compensator.

As the sad experience of the Hubble space telescope proves, the construction parameters in a lens compensator have to be very carefully measured and adjusted, otherwise an imperfect correction is

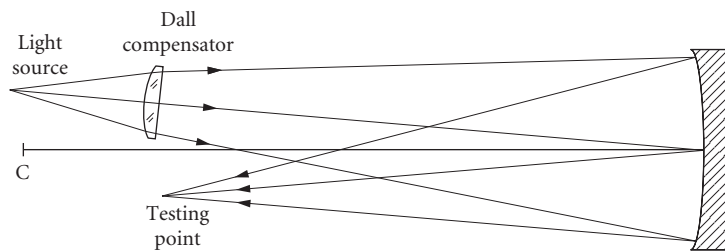


FIGURE 26 The Dall compensator.

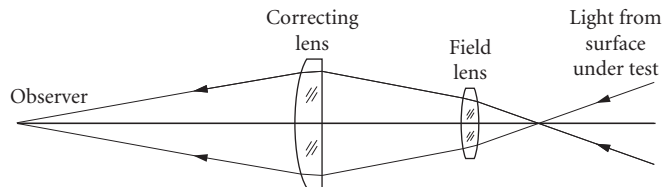


FIGURE 27 The Offner compensator. Only the reflected beam is shown.

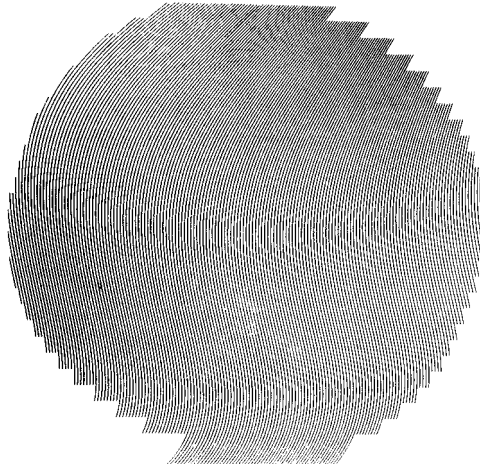


FIGURE 28 Computer-generated hologram for testing an aspherical wavefront. (From Wyant.³⁷)

obtained either by undercorrection or overcorrection. The distance from the compensator to the surface under test is one of those parameters to be carefully measured. A way around this problem would be to assume that the compensator detects smoothness imperfections but not the exact degree of asphericity. This degree of asphericity may then be measured with some independent measurement like the Hartmann test.

Holographic Compensators

Diffractional holographic elements also may be used to compensate the spherical aberration of the system and to obtain a null test. The hologram may be real, produced by photographing an interferometric pattern. This pattern has to be formed by superimposing on the screen a wavefront like the one we have to test and a perfectly flat or spherical wavefront. The only problem with this procedure is that a perfect wavefront with the same shape as the wavefront to be tested has first to be produced. This is not always easy.

A better approach is to simulate the holographic interference pattern in a computer,³⁶ as in Fig. 28. Then this image is transferred to a small photographic plate, with the desired dimensions. There are many experimental arrangements to compensate the aspherical wavefront aberration with a hologram. One of these is illustrated in Fig. 29.

Infrared Interferometry

Another simple approach to reduce the number of fringes in the interferogram is to use a long infrared wavelength. Light from a CO₂ laser has been used with this purpose. It can also be used when the surface is still quite rough.

Two-Wavelength Interferometry

In phase-shifting interferometry, each detector must have a phase difference smaller than π from the closest neighboring detector, in order to avoid 2π phase ambiguities and ensure phase continuity. In

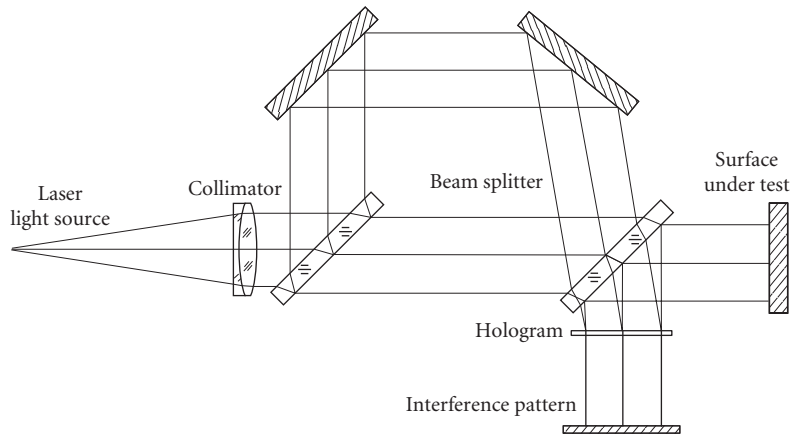


FIGURE 29 An optical arrangement for testing an aspherical wavefront with a computer-generated hologram.

other words, there should be at least two detector elements for each fringe. If the slope of the wavefront is very large, the fringes will be too close together and the number of detector elements would be extremely large.³⁷

A solution to this problem is to use two different wavelengths λ_1 and λ_2 simultaneously. The group wavelength or equivalent wavelength λ_{eq} is longer than any of the two components and is given by

$$\lambda_{eq} = \frac{\lambda_1 \lambda_2}{|\lambda_1 - \lambda_2|} \quad (34)$$

Under these conditions, the requirement in order to avoid phase uncertainties is that there should be at least two detectors for each fringe produced if the wavelength is λ_{eq} . The great advantage of this method is that we may test wavefronts with large asphericities, limited in asphericity by the group wavelength, and accuracy limited by the shortest wavelength of the two components.

Moiré Tests

An interferogram in which a large amount of tilt has been introduced is an ideal periodic structure to form moiré patterns. A moiré pattern represents the difference between two periodic structures. Thus, a moiré formed by two interferograms represents the difference between the two interferograms. There are several possibilities for the use in optical testing of this technique, as shown by Patorski.³⁸

Let us assume that the two interferograms are taken from the same optical system producing an aspherical wavefront, but with two different wavelengths λ_1 and λ_2 . The moiré obtained represents the interferogram that would be obtained with an equivalent wavelength λ_{eq} given by Eq. (31). If the tilt is of different magnitude in the two interferograms, the difference appears as a tilt in the moiré between them. Strong aspheric wavefronts may be tested with this method.

A second possibility is to produce the moiré between the ideal interferogram for an aspheric wavefront and the actual wavefront. Any differences between both would be easily detected.

Another possibility of application is for eliminating the wavefront imperfections in a low-quality interferometer. One interferogram is taken with the interferometer alone, without any optical piece under test. The second interferogram is taken with the optical component being tested. The moiré

represents the wavefront deformations due to the piece being tested, without the interferometer imperfections.

Sub-Nyquist Interferometry

It was pointed out before that in phase-shifting interferometry each detector must have a phase difference smaller than π from the closest neighboring detector, in order to avoid 2π phase ambiguities and to ensure phase continuity. In other words, there should be at least two detector elements for each fringe. This condition is known as the Nyquist condition.

Since there is a minimum practical distance between detectors, the maximum asphericity in a surface to be tested by phase-shifting interferometry is only a few wavelengths. This condition may be relaxed³⁹ if the wavefront and its slope are assumed to be continuous on the whole aperture. Then, optical surfaces with larger asphericities may be tested.

Wavefront Stitching

When an aspheric and a flat reference wavefronts interfere, the fringe spacing is minimum where the angle between the two wavefronts is larger. When the aspheric wavefront has rotational symmetry and there is no angle between them (no tilt) near the optical axis, the minimum fringe spacing occurs at the edge of the pupil. The maximum fringe spacing is at the center, where the two wavefronts are parallel to each other.

Most times the fringe pattern is imaged on a CCD detector with a rectangular array of small square pixels. According to the Nyquist sampling condition, the fringes can be detected only if the detector has more than two pixels per fringe spacing. With strongly aspheric wavefronts this condition can not be satisfied near the pupil edge.

If the flat reference wavefront is tilted or made slightly spherical, the zone of the interferogram with maximum fringe spacing can be located at any desired. Then the interferogram can be measured at a zone around this point with maximum fringe spacing where the Nyquist condition is satisfied. By moving this point the whole interferogram can thus be measured in small pieces. Then, all pieces should be joined together in a process called wavefront stitching,⁴⁰ as illustrated in Fig. 30.

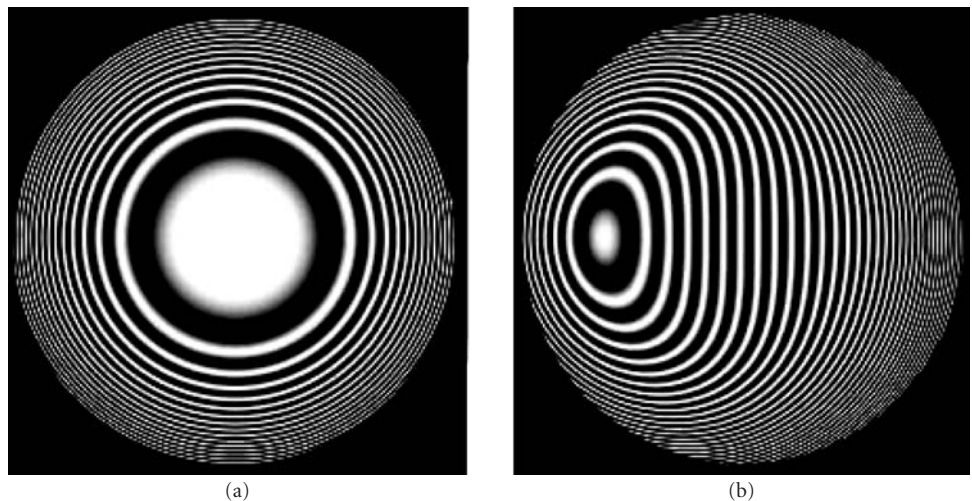


FIGURE 30 Two different interferograms of the same wavefront with different tilts to do wavefront stitching.

13.9 REFERENCES

1. D. Malacara, *Optical Shop Testing*, 3d ed., John Wiley and Sons, New York, 2007.
2. L. M. Foucault, "Description des Procédes Employes pour Reconnaître la Configuration des Surfaces Optiques," *C.R. Acad. Sci. Paris* **47**:958 (1852); reprinted in Armand Colin, *Classiques de al Science*, vol. II.
3. J. Ojeda-Castañeda, "Foucault, Wire and Phase Modulation Tests," in D. Malacara (ed.), *Optical Shop Testing*, 3d ed., John Wiley and Sons, New York, 2007.
4. V. Ronchi, "Le Franque di Combinazione Nello Studio Delle Superficie e Dei Sistemi Ottici," *Ri. Ottica mecc. Precis.* **2**:9 (1923).
5. J. Hartmann, "Bemerkungen über den Bann und die Justirung von Spektrographen," *Zt. Instrumentenk.* **20**:47 (1900).
6. B. C. Platt and R. V. Shack, "Lenticular Hartmann Screen," *Opt. Sci. Newsl.* **5**: 15–16 (1971).
7. D. Malacara, *Interferogram Analysis for Optical Testing*, 2d ed., CRC Press, Taylor and Francis Group, Boca Raton, FL, 2005.
8. R. N. Smart and J. Strong, "Point Diffraction Interferometer," (Abstract only) *J. Opt. Soc. Am.* **62**:737 (1972).
9. C. Roychoudhuri, "Multiple-Beam Interferometers," in D. Malacara (ed.), *Optical Shop Testing*, 3d ed., John Wiley and Sons, New York, 2007.
10. P. Hariharan and D. Sen, "The Separation of Symmetrical and Asymmetrical Wave-Front Aberrations in the Twyman Interferometer," *Proc. Phys. Soc.* **77**:328 (1961).
11. P. Hariharan, "Multiple-Pass Interferometers," in D. Malacara (ed.), *Optical Shop Testing*, 2d ed., John Wiley and Sons, New York, 1991.
12. F. Zernike, "Diffraction Theory of Knife Edge Test and Its Improved Form: The Phase Contrast," *Mon. Not. R. Astron. Soc.* **94**:371 (1934).
13. D. Rozenzweig and B. Alte, "A Facility for the Analysis of Interferograms," in A. H. Guenther, D. H. Liedbergh (eds), *Optical Interferograms—Reduction and Interpretation*, ASTM Symposium, *Am. Soc. for Test and Mat. Tech.* Publ. 666, West Consohocken, PA, 1978.
14. K. H. Womack, J. A. Jonas, C. L. Koliopoulos, K. L. Underwood, J. C. Wyant, J. S. Loomis, and C. R. Hayslett, "Microprocessor-Based Instrument for Analysis of Video Interferograms," *Proc. SPIE* **192**:134 (1979).
15. G. T. Reid, "Automatic Fringe Pattern Analysis: A Review," *Opt. and Lasers in Eng.* **7**:37 (1986).
16. G. T. Reid, "Image Processing Techniques for Fringe Pattern Analysis," *Proc. SPIE* **954**:468 (1988).
17. D. Malacara, J. M. Carpio-Valadéz, and J. J. Sánchez-Mondragón, "Wavefront Fitting with Discrete Orthogonal Polynomials in a Unit Radius Circle," *Opt. Eng.* **29**:672 (1990).
18. C. R. Hayslett and W. Swantner, "Wave Front Derivation from Interferograms by Three Computer Programs," *Appl. Opt.* **19**:3401 (1980).
19. F. Becker, G. E. A. Maier, and H. Wegner, "Automatic Evaluation of Interferograms," *Proc. SPIE* **359**:386 (1982).
20. F. Zernike, "Begünstheorie des Schneidener-Fahrens und Seiner Verbasserten Form, der Phasenkontrastmethode," *Physica* **1**:689 (1934).
21. K. H. Womack, "Frequency Domain Description of Interferogram Analysis," *Opt. Eng.* **23**:396 (1984).
22. W. W. Macy, Jr., "Two Dimensional Fringe Pattern Analysis," *Appl. Opt.* **22**:3898 (1983).
23. M. Takeda, H. Ina, and S. Kobayashi, "Fourier Transform Method of Fringe-Pattern Analysis for Computer-Based Topography and Interferometry," *J. Opt. Soc. Am.* **72**:156 (1982).
24. C. Roddier and F. Roddier, "Interferogram Analysis Using Fourier Transform Techniques," *Appl. Opt.* **26**:1668 (1987).
25. J. H. Bruning, D. J. Herriott, J. E. Gallagher, D. P. Rosenfeld, A. D. White, and D. J. Brangaccio, "Digital Wavefront Measurement Interferometer," *Appl. Opt.* **13**:2693 (1974).
26. J. Greivenkamp and J. H. Bruning, "Phase Shifting Interferometers," in D. Malacara (ed.), *Optical Shop Testing*, 2d ed., John Wiley and Sons, New York, 1991.
27. K. Creath, "Phase-Measurement Interferometry Techniques," in E. Wolf (ed.), *Progress in Optics*, vol. XXVI, Elsevier Science Publishers, Amsterdam, 1988.

28. P. L. Wizinowich, "Systems for Phase Shifting Interferometry in the Presence of Vibration: A New Algorithm and System," *Appl. Opt.* **29**:3271–3279 (1990).
29. K. Freischlad and C. L. Koliopoulos, "Fourier Description of Digital Phase Measuring Interferometry," *J. Opt. Soc. Am. A*. **7**:542–551 (1990).
30. N. Bareket, "Three-Channel Phase Detector for Pulsed Wavefront Sensing," *Proc. SPIE* **551**:12 (1985).
31. C. L. Koliopoulos, "Simultaneous Phase Shift Interferometer," *Proc. SPIE* **1531**:119–127 (1991).
32. N. A. Massie, "Digital Heterodyne Interferometry," *Proc. SPIE* **816**:40 (1987).
33. G. W. Johnson, D. C. Leiner, and D. T. Moore, "Phase Locked Interferometry," *Proc. SPIE* **126**:152 (1977).
34. G. W. Johnson, D. C. Leiner, and D. T. Moore, "Phase Locked Interferometry," *Opt. Eng.* **18**:46 (1979).
35. D. T. Moore, "Phase-Locked Moire Fringe Analysis for Automated Contouring of Diffuse Surfaces," *Appl. Opt.* **18**:91 (1979).
36. J. C. Wyant, "Holographic and Moire Techniques," in D. Malacara (ed.), *Optical Shop Testing*, John Wiley and Sons, New York, 1978.
37. J. C. Wyant, B. F. Oreb, and P. Hariharan, "Testing Aspherics Using Two-Wavelength Holography: Use of Digital Electronic Techniques," *Appl. Opt.* **23**:4020 (1984).
38. K. Paturski, "Moire' Methods in Interferometry," *Opt. and Lasers in Eng.* **8**:147 (1988).
39. J. E. Greivenkamp, "Sub-Nyquist Interferometry," *Appl. Opt.* **26**:5245 (1987).
40. J. Liesener and H. Tiziani, "Interferometer with Dynamic Reference," *Proc. SPIE* **5252**:264–271 (2004).

